Al-Mhana T, Pickert V, Atkinson DJ, Zahawi B.

Forced Commutated Controlled Series Capacitor Rectifier for More Electric Aircraft.

***IEEE Transactions on Power Electronics* 2018**

DOI: https://doi.org/10.1109/TPEL.2018.2816305

Forced Commutated Controlled Series Capacitor Rectifier for More Electric Aircraft

Tahani Al-Mhana, Volker Pickert, *Member, IEEE*, David J. Atkinson, and Bashar Zahawi, *Senior Member, IEEE*

***Abstract*—Rising power demands in More Electrical Aircraft (MEA) put power converters for commercial airplanes under increasing pressure to fulfill current harmonic distortion regulations as specified, for example, in DO-160G. Today, the implementation of filters is seen as an effective tool for dealing with harmonics, however, their increased weight and volume is not welcomed in the aerospace industry. This paper proposes a circuit, named Forced Commutation Series Capacitor rectifier (FCSC-rectifier), which is able to maintain low individual harmonic current levels without the need for filter components. The FCSC-rectifier includes a variable capacitive line reactance that interacts in a controlled manner with the inductive line impedance. The result is that the converter input current is nearly purely sinusoidal with a power factor of almost unity. The FCSC-rectifier is to be used for stand-alone variable-voltage, variable-frequency generation systems (VFG) and can therefore power the Full Authority Digital Electronic Control System (FADEC) in an MEA. This paper shows that the FCSC-rectifier can maintain a high power factor and acceptable current harmonic levels without the use of filters, despite large voltage and frequency variations. A full description of the circuit modes of operation is presented in this paper together with simulation results showing circuit performance characteristics over a range of voltages and frequencies. Results are experimentally verified using a 1kW test circuit.**

***Index Terms*— Forced Commutated controlled Series Capacitor (FCSC), Full Authority Digital Electronic Control System (FADEC), More Electric Aircraft (MEA), current harmonics, power factor.**

I. Introduction

The complexity of aircraft electrical loads has substantially increased in recent years with the advent of the More Electric Aircraft (MEA) [1-3]. The most safety critical system in any MEA is the FADEC (Full Authority Digital Electronic Control) system that continuously monitors and controls the ignition timing and fuel injection to the aircraft engine. FADEC control and designs have been reported in [4-6] with the focus being mainly on safety. Any failure within the FADEC leads to misfiring and loss of fuel injection [7-10] which would result in a catastrophic event, such as the Airbus A 400M crash in 2015 caused by FADEC failure [11]. One major area of concern is radiated and conducted EMI which could interact with the engine control

T. Al-Mhana, V. Pickert and D. J. Atkinson are with the School of Engineering, Newcastle University, Newcastle upon Tyne NE1 7RU, UK (e-mail: volker.pickert@ncl.ac.uk).

B. Zahawi is with the Department of Electrical and Computer Engineering, Khalifa University, Abu Dhabi 127788, United Arab Emirates (e-mail: bashar.zahawi@ku.ac.ae).

hardware. Radiated EMI is minimized by enclosing the FADEC in a metal cage. Conducted EMI is minimized by powering the FADEC from its own variable frequency generator (VFG), minimizing the risk of harmonic contamination from the supply currents when connected to the MEA distribution network. The FADEC is the only stand-alone powered electronic system that has its own VFG in the MEA (there is, however, a dc link connection to a back-up system which is activated in case of the loss of the VFG [12]). As well as producing low harmonics, the VFG must also be reliable, low-cost, power-dense, light in weight and environmental friendly [13-15], as is necessary for all MEA electronic systems.

Today's standard VFG design for FADEC supplies is the series connection of a permanent magnet (PM) generator with a diode bridge rectifier and a dc/dc converter stepping down the voltage to 28 V. The dc/dc converter is designed to cope with load variations caused by the FADEC although variations are small as digital controller boards do not experience large load swings. This principal was proposed in 2009 [12] and is still implemented in todays most advanced MEAs such as the Airbus A 380 and Boing 787. The combination of a PM generator and a diode bridge rectifier fulfills aerospace requirements in that it is efficient, power-dense and reliable [16-18]. However, the PM generator/diode bridge rectifier combination is known for its current harmonic generation and poor power factor [19].

So far this has not been an issue, as the power requirement of the FADEC hardware is relatively low. Future aircraft, however, will have more complex engines with more electronic hardware and processing needs, requiring higher levels of input power. This, in addition to further increases in the electrification regulatory requirements for commercial aircrafts, such as those specified in DO-160G "Environmental Conditions and Test Procedures for Airborne Equipment," imposed by the Radio Technical Commission for Aeronautics (RTCA) [20], will push the limits of acceptable current harmonic levels.

The DO-160G is a guideline for the standard procedures and criteria of environmental tests for airborne hardware, including electrical and electronic avionics and mechanical systems. It also defines the input harmonics distortion limits caused by various loads, due to the recognition of the negative impact of harmonics on aircraft power systems caused mainly by the intensive use of uncontrolled rectifiers in airborne systems. Historically, DO-160G has been updated regularly in line with developments in the MEA industry and PM generators with diode bridge rectifiers are likely to be prohibited in the future due to the ever-tighter limitations on power converter current harmonic distortion

Consequently, alternative solutions are required for powering stand-alone electrical systems in MEA such as the FADEC. The most obvious approach is the implementation of filters between the PM generator and the diode bridge rectifier. However, this will increase the volume and weight of such a system by about 50% [21] which is not desirable. Other work has focused on the employment of passive and active three-phase high power factor converter topologies [22-25]. The use of a transformer rectifier unit [26] or an autotransformer rectifier unit [27] has been investigated to supply a multi-pulse (12- or 18-pulse) rectified DC voltage. These rectifier units are adapted for current harmonic cancellation to meet DO-160G requirements but at the expense of

increased weight and volume [28]. The use of well-established active rectifiers such as the two- and multi-level pulse width modulation rectifier, and Vienna rectifier have also been investigated [29- 31]. Although these are able to enhance the power factor without the use of transformers, the control circuit complexity raises safety concerns and the high-power, fast switching requirements result in current harmonics that still require filtering [19, 28, 30]. Current harmonics produced by active front-end converters are determined by many factors such as: load, switching frequency, filter design, type of filter and PWM control strategy [32-33]. A summary of all rectifiers proposed in the literature as an alternative to the diode bridge rectifier is presented in Fig. 1.

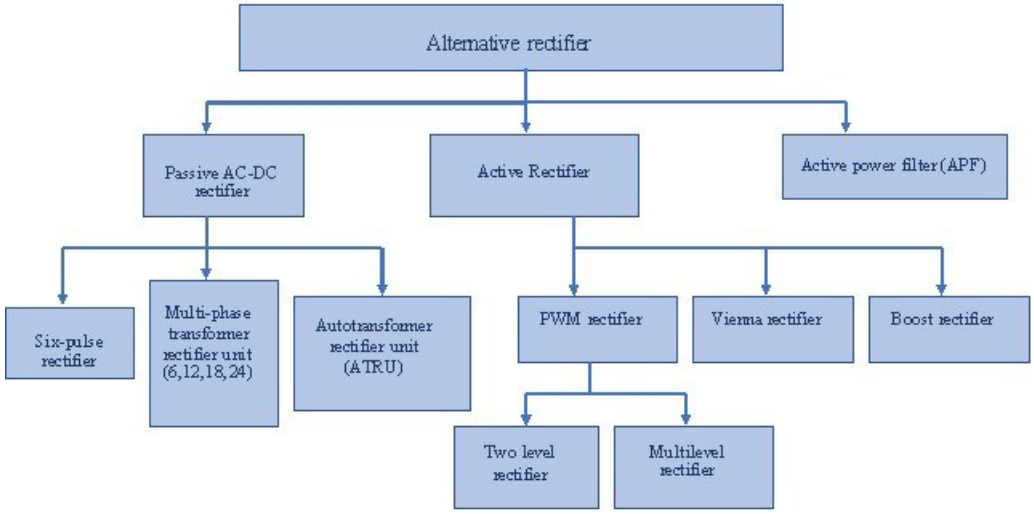

Fig. 1. Overview of rectifiers presented in the literature as an alternative to the diode bridge rectifier.

To-date, all proposed systems for current harmonic reduction require filtering or additional magnetic components. This paper proposes a power electronic rectifier circuit that produces low current harmonics, fulfilling DO-160G requirements without the need for filters. The new rectifier circuit is referred to in this paper as the Forced Commutation controlled Series Capacitor rectifier (FCSC-rectifier). It has a simple control structure and it operates at a low switching frequency to produce a nearly sinusoidal supply current waveform at a power factor of almost unity. The operation of the proposed FCSC-rectifier is described, simulated and experimentally verified using a 1 kW test circuit.

The remainder of the paper is structured as follows: Section II describes the fundamental principal of the FCSC-rectifier topology. In Section III, the modes of operation of the FCSC-rectifier are presented, including a description of the control method that has been applied. Simulations using Saber/Synopsys are presented in Section IV. The FCSC-rectifier behavior is verified experimentally using a 1 kW laboratory test bench and test waveforms and results are shown in Section V. Current harmonic spectrums (experimental and simulated waveforms) are shown in Section VI and a conclusion is presented in Section VII.

II. FCSC-RECTIFIER CIRCUIT TOPOLOGY

The FCSC-rectifier is shown in Fig. 2, situated between the aircraft three-phase PM generator and the on-board DC load (shown

in the figure as an equivalent resistor). The three-phase FCSC-rectifier is comprised of a three-phase, forced commutation controlled capacitor circuit in series with a three-phase diode bridge rectifier. In each phase, a series compensation capacitor C_c is connected in parallel to two anti-parallel IGBT switches used to control the injected series capacitive reactance. The aim is to match the effective capacitive reactance with the generator inductive reactance to achieve high power factor and minimum current distortion for a wide range of operating frequencies, thus avoiding the need for additional filtering.

The FCSC-rectifier is based on the topology used in FACTS (Flexible AC Transmission System) controllers in power system applications, where AC voltages and frequencies are generally stable [34-36]. The purpose of the FCSC circuit in FACTS applications is to inject a small capacitive reactance into the transmission lines for grid quality purposes [37, 38]. The IGBTs are switched-on at the zero-crossing point of the supply voltage and the turn-off time is calculated based on the required amount of injected capacitive reactance.

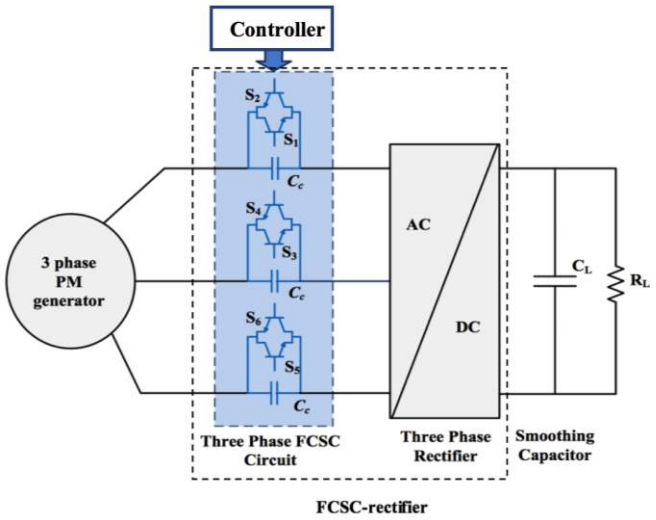

Fig. 2. Three-phase FCSC-rectifier in a stand-alone three-phase generation system.

The proposed FCSC-rectifier is different from the FACTS conventional circuit in several ways. Firstly, it is designed for stand-alone applications, embedded between an AC generator and a DC output stage. Secondly, an AC current is injected into the rectifier as the effective capacitive reactance can be controlled by varying the on-state time of the IGBT switches and resonance is achieved by tuning the phase capacitive reactance to the same value of the inductive reactance of the PM generator. This operational point has two advantages: a near sinusoidal AC current waveform with low current harmonics and a high input power factor, as the current is in phase with the generator phase-voltage. It is perhaps worth noting that the operation of the input stage of the FCSC-rectifier cannot be compared directly with a classical RLC resonant circuit. This is because the series capacitor C_c is switched via the action of the IGBTs and the voltage across the capacitor is not always part of the series resonant circuit formed by the generator inductance, generator resistance and C_C. Thirdly, FCSCs in FACTS applications operate with small AC input variations (typically ±1% variation of nominal frequency and ±10% of nominal voltage) [39] whereas the FCSC-rectifier has to deal with the full range

of output voltage fluctuation and frequency variation produced from the VFG. As the operation of the FCSC-rectifier is fundamentally different to that of the FCSC, the control strategy must also be different. This is discussed in the following section.

III. Modes of Operation and Control Method

Fig. 3 shows a three-phase FCSC-rectifier with its input connected to the three-phase generator and its output connected to a load capacitor C_L in parallel with a load resistor R_L. In this figure, the three-phase PM generator is represented by a set of balanced three-phase voltage sources (*va*, *vb*, *vc*), in series with three identical impedances (internal resistance R_s and inductance L_s) in each phase. The phase voltages in this balanced three-phase system are given by:

$$v_a = V_{max}\sin(\omega t)$$
$$v_b = V_{max}\sin(\omega t - 2\pi/3) \quad (1)$$
$$v_c = V_{max}\sin(\omega t - 4\pi/3)$$

where V_{max} is the amplitude of the sinusoidal generator induced voltage.

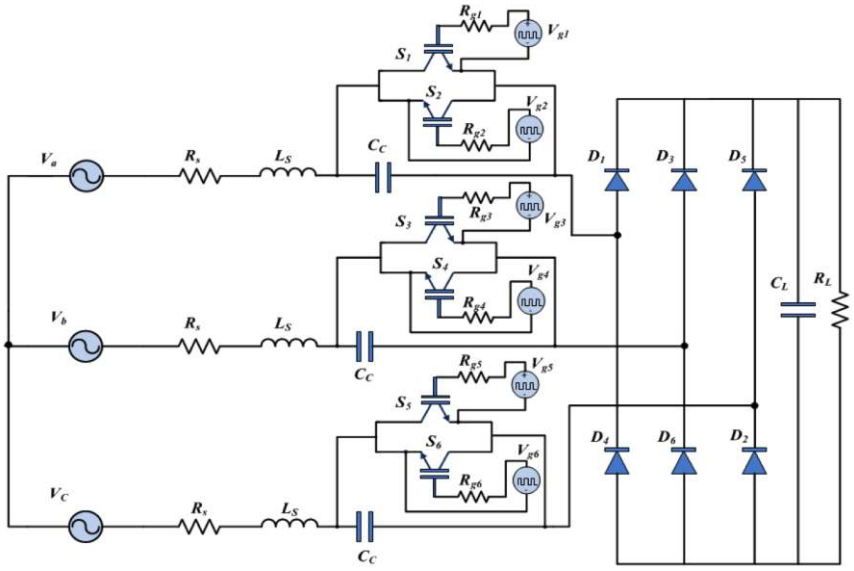

Fig. 3. Schematic diagram of the three-phase FCSC-rectifier.

Each phase includes a series connected compensation capacitor C_C whose value is chosen in accordance with the generator inductance to insure resonance at the maximum operating supply frequency (f_{max}) [40]:

$$f_{max} = f_r = \frac{1}{2\pi\sqrt{L_S C_C}} \quad (2)$$

where f_r is the resonance frequency. The value of C_c can then be determined from the following formula:

$$X_{CC}|_{f_S=f_{max}} = X_{cmax} = \frac{1}{2\pi \times f_{max} \times C_c} \quad (3)$$

Resonance can be achieved by controlling the duty ratio of the IGBT switches in accordance with the supply frequency value.

When the operating frequency is reduced, the controller increases the duty ratio of the switches (the capacitor is bypassed by the IGBTs for a longer period) and the effective capacitive reactance $X_{cc,eff}$ is reduced [41] in line with the reduction in X_{LS} maintaining the condition:

$$X_{CC,eff} = X_{LS} = \omega L_S \quad (4)$$

where ω is the electric angular frequency produced by the generator.

X_{CC_eff} is determined by the capacitor C_C and the conduction period δ of the associated IGBTs. The duty ratio (D) for each active switch can be calculated as:

$$D = \frac{\delta}{2\pi} \quad (5)$$

In one full cycle, the capacitor will be short-circuited twice by the corresponding pair of IGBT switches. The effective capacitive reactance is then given by:

$$X_{cc,eff} = (1 - 2D) \times X_{cmax} \quad (6)$$

by substituting (4) in (6), we obtain:

$$X_{LS} = (1 - 2D) \times X_{cmax} \quad (7)$$

Equation (7) can be re-written as:

$$D = \frac{1}{2}\left(1 - \frac{X_{LS}}{X_{Cmax}}\right) \quad (8)$$

Giving the relationship:

$$D = \frac{1}{2}(1 - \frac{f_s}{f_{max}}) \quad (9)$$

The duty cycle D for each frequency variation is calculated using (9). In the practical implementation of the circuit, the microcontroller calculates the new duty-cycle based on the frequency f_s of the previous cycle. The frequency f_s is determined using a zero-crossing detection (ZSD) circuit and therefore the ZSD triggers the calculation of the conduction period δ which can be calculated from equations (5) and (9):

$$\delta = \pi(1 - \frac{f_s}{f_{max}}) \quad (10)$$

Thus, all switches are synchronized to the ZSD trigger event and therefore the FCSC-rectifier only requires a low-cost microcontroller to deal with MEA's variable frequency generator range. By applying the correct duty cycle, the resonance condition expressed in (4) is achieved and the generator current waveform is maintained in-phase with the generator voltage waveform resulting in almost unity power factor operation.

Fig. 4 displays the timing diagram and the various modes of operation of the circuit, showing the diode conducting periods together with the switching patterns of all IGBT switches. During the positive half-cycles of the three-phase generator voltage, switches S_1, S_3 and S_5 are ON (and during the negative half-cycle S_2, S_4 and S_6 are ON) for an interval δ that is symmetrically centered around the peak of the generator voltage waveform.

Each IGBT has a conduction period of δ which can vary from δ=0 to δ=π/2. The IGBT ON time is varied in line with the supply frequency variations. At resonance, each phase produces a pure sinusoidal AC current waveform:

$$i_a = I_{max}\sin(\omega t)$$
$$i_b = I_{max}\sin(\omega t - 2\pi/3) \qquad (11)$$
$$i_c = I_{max}\sin(\omega t - 4\pi/3)$$

where I_{max} is the amplitude of the sinusoidal phase current.

Fig. 4 shows the total current is always zero because the system is balanced. The state of conduction of the diodes depends on the direction of the phase currents (the upper diodes D_1, D_3, D_5 conduct when the corresponding phase current is positive and the lower diodes D_2, D_4, D_6 conduct when the current is negative). As the FCSC-rectifier operates on the basis of phase current injection when running at resonance, the diode commutation process is different from that found in classical voltage-fed rectifiers. In the latter, commutation takes place between neighboring diodes (from one conducting leg to the neighboring leg). In the FCSC-rectifier, however, diode commutation always takes place between the upper and the lower diodes in the same leg, resulting in the six-pulse DC current waveform shown in Fig. 5, in which the operation of the FCSC-rectifier is compared with that of a conventional three-phase diode bridge rectifier.

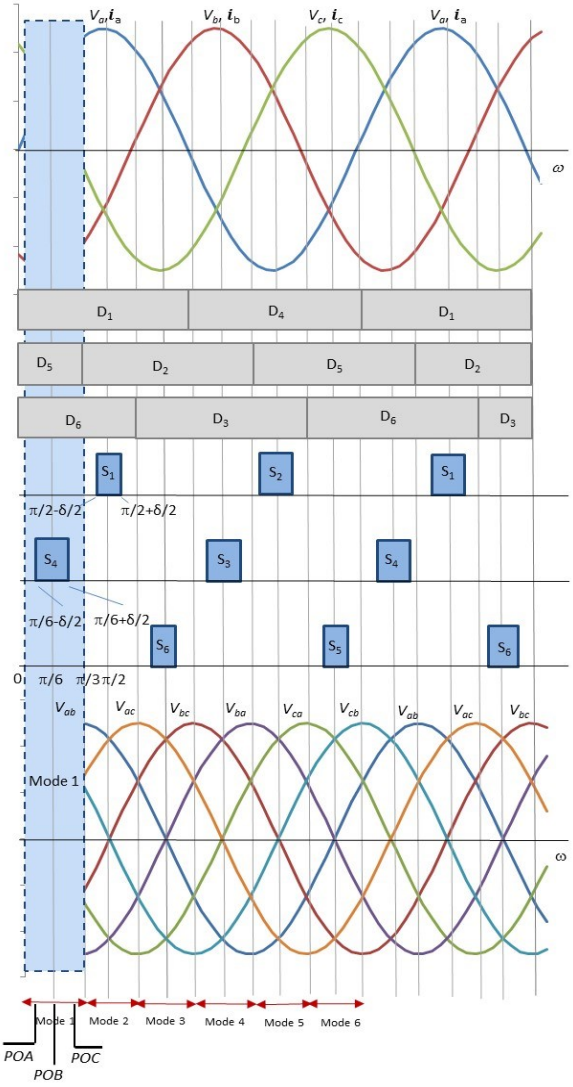

Fig. 4. Operational modes, switching states, and normalized voltage and current waveforms of the three-phase FCSC-rectifier.

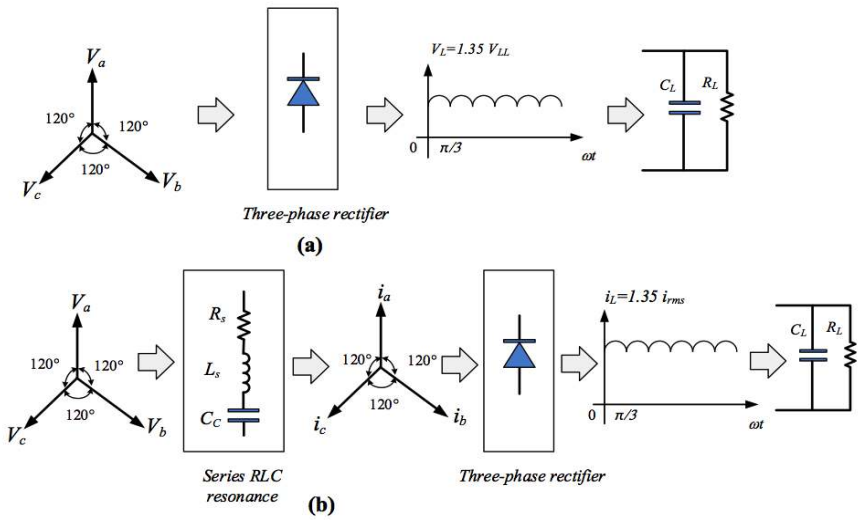

Fig. 5. Comparison of operating characteristics: (a) Classical voltage-fed rectifier, (b) FCSC-rectifier.

Each mode shown in Fig. 4 (Modes 1 to 6) lasts for a period of π/3 and corresponds to a given diode conduction pattern. Due to symmetry, each mode has the same repeating principal operations (referred to here as POA, POB, and POC). These are discussed below for Mode 1:

A. Principal Operation A (POA): $0<\omega t<\pi/6-\delta/2$: D_1, D_5 and D_6 conduct

Fig. 6 shows the circuit at the start of Mode 1. In this figure, the R_L-C_L load is represented as a single unit for simplicity. Mode 1 starts at ωt=0 (using v_a as a reference, as shown in Fig. 4). At the start of this period, no switch has been activated and diodes D_1, D_5 and D_6 are conducting. As the effective overall capacitive reactance X_{cc_eff} over the full cycle is equal to X_{LS}, the currents i_a, i_b, and i_c are in phase with the voltages v_a, v_b and v_c, respectively. In this mode, i_a and i_c are positive flowing into the diode bridge rectifier and i_b is negative (Fig. 4). The currents i_a, i_b, and i_c are given by (12) and the load current I_L can be determined from Kirchhoff's current law:

$$I_L = ia + ic = I_{max}\sin(\omega t - 2\pi/3) \quad (12)$$

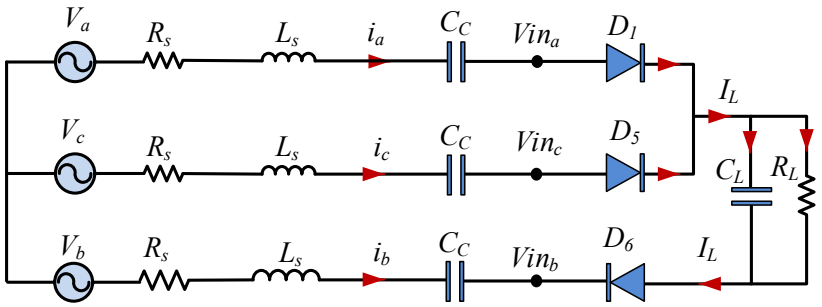

Fig. 6. Effective circuit during POA

B. Principal Operation B (POB): $\pi/6-\delta/2<\omega t\pi/6+\delta/2$: S_4 ON, D_1, D_5 and D_6 conduct

At ωt=π/6-δ/2, S_4 is turned ON and all other IGBTs are OFF (Fig. 7). S_4 is ON during this period, short circuiting C_C in phase-b. However, since $X_{cc,eff}$ is still adjusted over the full cycle to be equal to X_{LS}, i_a and i_c are still in phase with v_a and v_c, respectively, and phase b provides the return path for i_a and i_c:

$$i_b = -ia - ic \quad (13)$$

Despite the short-circuiting of the capacitor C_C in phase-b, a resonant current is injected in phase-b which is in phase with the voltage v_b (Fig. 4). The load current I_L can still be determined from Kirchhoff's current law and equation (12).

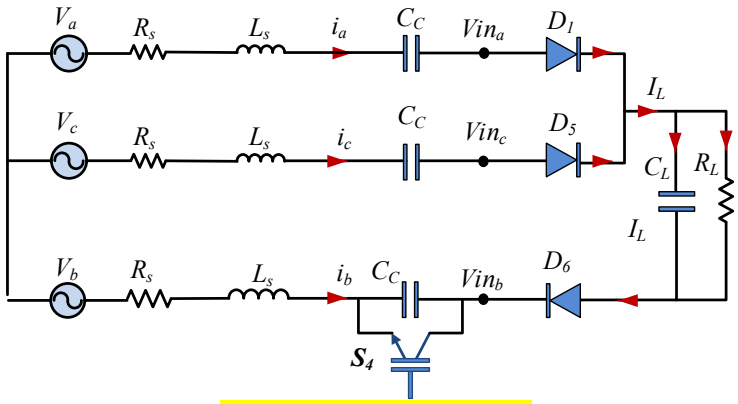

Fig. 7. Effective circuit during POB

C. Principal Operation C (POC): π/6+δ/2<ωt<π/3: D_1, D_2 and D_6 conduct

At ωt = π/6+δ/2, S4 is turned OFF and all remaining IGBTs are off. The circuit is identical to that shown in Fig. 6 and circuit operation is identical to POA.

At ωt=π/3 Mode 2 starts as v_c becomes negative and the current in phase-c changes polarity. The current in diode D_5 commutates to D_2, as shown in Fig.4.

IV. Simulation Results

To allow for direct comparisons with experimental tests, the FCSC-rectifier circuit is simulated in Saber using the parameters of the experimental test rig listed in Table 1. Generator parameters are based on an aero engine generator described in [42, 43]. The simulations are carried out for a frequency/voltage range between (240-480 Hz)/(75-100 V) to comply with the minimum/maximum frequency/voltage of the programmable power source used in the practical test. At the maximum frequency of 480 Hz, with a voltage of 100 V, all the IGBT switches are permanently OFF. Below this frequency the IGBTs are controlled to obtain a conduction period δ based on (15). Fig. 8 shows a summary of steps required to calculate the IGBTs on and off times. Fig. 9 shows the high level block diagram of the circuit simulation model.

Table 1. Circuit parameters

Circuit parameter	Value
V_S	75 V-100 V
f_S	240 Hz-480 Hz
Rs	2.5 Ω
L_s	13.75 mH
C_C	8 μF
C_L	500 μF
R_L	30 Ω

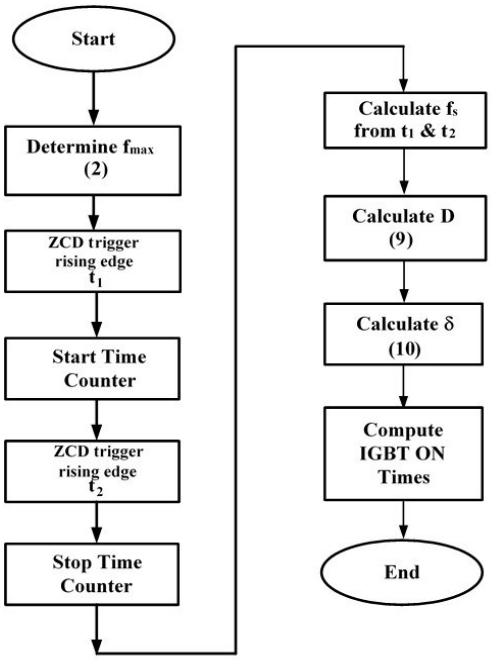

Fig. 8. Flow chart for computing IGBT switching times (t_1: timing when supply voltage crosses zero, t_2: timing when supply voltage crosses zero for the second time)

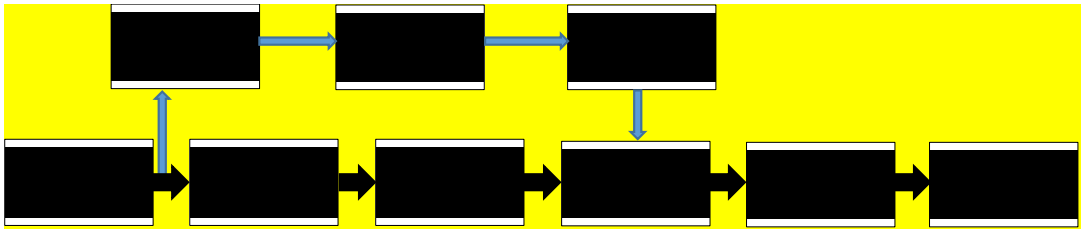

Fig. 9. Block diagram of circuit simulation model (black arrows: power, blue arrows: signal)

Simulation results for the FCSC-rectifier operating at a typical aircraft frequency of 400 Hz (also known as the nominal frequency [13, 30]) are shown in Fig. 10. The figure shows that the series capacitor can maintain the input current in-phase with the voltage waveform, so that the power factor is maintained at a high value. The rectifier input voltage V_{in} is clamped by the load voltage and the rectifier output current (i_L) consists of six pulses of the AC phase currents, as described in Section III. The average DC load current also complies with the relationship I_L= 1.35 I_{RMS}. The voltage across the series capacitor is zero as long as the corresponding IGBTs are in the ON state.

Fig. 11 shows the operating power factor of the circuit plotted against variations in load for 3 different voltage/frequency conditions. The FCSC-rectifier maintains a high power factor for all voltage/frequency values with a minimum value of 0.99. The highest power factor of 0.998 is achieved at the highest voltage/frequency values (100V/ 480Hz) under heavy load conditions and the lowest power factor occurs at the lowest voltage/frequency values (75V/240Hz) under light load conditions. The output

capacitor C_L represents the input stage of a dc/dc converter that would normally be connected to the output of the diode bridge rectifier of the FADEC and is therefore simulated as a constant value. Unlike in a classical diode bridge rectifier where C_L experiences periodical current charging spikes flowing from the AC supply C_L in the FCSC-rectifier experiences a six-pulse dc current waveform as shown in Fig. 10. Each pulse lasts for 60 degrees independently of the input frequency and the load. Changes in C_L values have no noticeable impact on the operation of the circuit but will affect the ripple content of load voltage and load current.

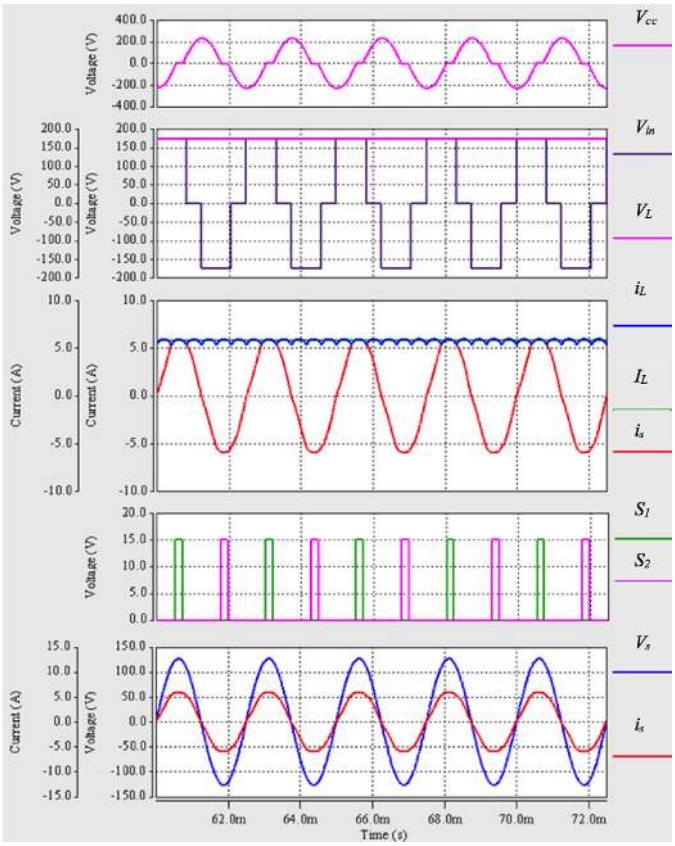

Fig. 10. Three-phase FCSC-rectifier waveforms at 90V/400 Hz (simulated). V_{cc}: voltage across the capacitor, V_{in}: line-to-line input voltage of the three-phase rectifier (diode bridge), V_L: load voltage, I_L: load current, i_L: output current of the three-phase rectifier, i_S: supply current, V_s: supply voltage.

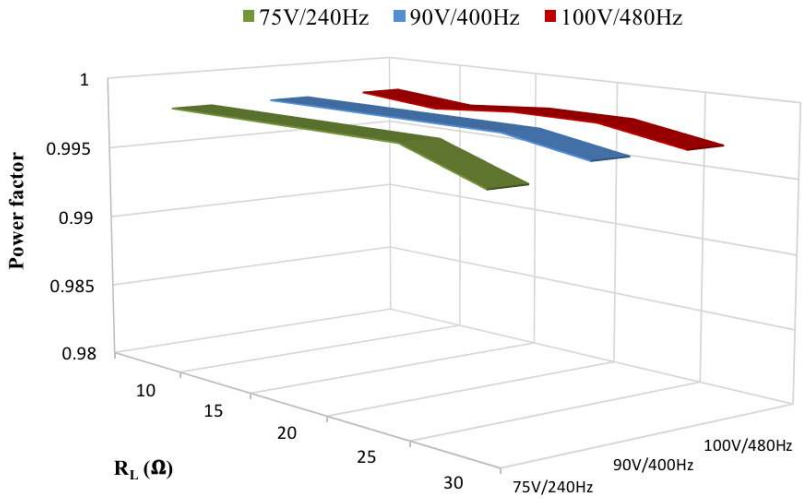

Fig. 11. FCSC-rectifier power factor as a function of PM generator voltage and frequency under various load conditions (simulated results).

A sensitivity study (Table 2) and a study of unbalanced operation (Table 3) was conducted for 100V/480Hz operation at two load conditions: full load R_L=*10 Ω* and half load R_L=*20 Ω*. In the sensitivity analysis, a 10% error in the values of either L_s or C_C was applied to all three phases. For unbalanced operation, a 10% imbalance in the values of either L_s or C_C was considered as well as an imbalance in the supply voltages (v_a=100 V, v_b=120 V and v_c=110 V).

Table 2. Sensitivity study

Load	10% error in	PF-10%	PF
R_L=10Ω	L_S	0.902	0.997
	C_C	0.916	0.997
R_L=20Ω	L_S	0.962	0.998
	C_C	0.968	0.998

Table 3. Unbalanced operation

Load	10% imbalance in	PF-10%	PF
R_L=10Ω	L_S	0.963	0.997
	C_C	0.961	0.997
R_L=20Ω	L_S	0.937	0.998
	C_C	0.918	0.998

The third column (PF-10%) in both tables shows the resulting PF values, whereas the values in the fourth column are the PFs with no errors or imbalances. Errors and imbalances clearly reduce the PF values that could be achieved, but they do not alter the fundamental operation of the circuit. Table 2 shows that the highest drop in PF (from 0.997 to 0.902) is at R_L=10 Ω and a 10% error in L_s. The highest drop in PF in Table 3 (from 0.998 to 0.918) is at R_L=20 Ω and a 10% imbalance in C_C. Generator voltages

imbalance (v_a=100 V, v_b=120 V and v_c=110 V) produced no measurable change in PF. This is because the displacement factor is independent of the voltage supply amplitude.

V. EXPERIMENTAL VALIDATION

The behavior of the three-phase FCSC-rectifier was experimentally verified under various operating conditions using a 1 kW laboratory test bench. A photograph of the test bed is shown in Fig. 12. All recorded AC measurements were captured for phase-*a* only. The test hardware consisted of three major parts. The PM generator was emulated using 60 KVA Behlman programmable AC power supply with an internal inductive and resistive impedance to emulate the PM generator. This power supply was used to provide the system with variable-voltage and variable-frequency power over a frequency range between (240-480 Hz). The second part is the conversion stage (inside the enclosure) including the three-phase FCSC-rectifier. Three dual-gate driver circuits were used to provide the pulses required to drive the IGBT switches. The voltage and current sensor cards were also placed inside the enclosure with the zero-crossing detection (ZCD) card, as shown in Fig. 13. The ZCD circuit is shown in Fig. 14. It includes an RC low-pass filter to prevent spurious zero crossing detections caused by the AC source distortion (22 nF and 390 Ω resistor). An LM393N comparator is used to produce the square wave output voltage signal by comparing the filtered voltage signal with a reference voltage. A 100 kΩ potentiometer was provided in order to adjust the pulse width as required. The readings of the current sensors and the ZCD card were fed to the microcontroller to be processed. Finally, the controller was based on a TMS320F28335 Texas Instruments DSP mounted on a general interface board. A host computer was required to provide an environment in which to debug the software. A National Instruments LabView package was used for monitoring and control purposes. The resistive load was fed from the output of the three-phase rectifier. Table 4 summarizes the specifications of the experimental test rig and the main components of the FCSC-rectifier. The total volume of the power components used in the test circuit is 1090.85 cm3 and the weight (without heatsink) is 931.3 g.

Table 4. Experimental rating specification and components of the FCSC-rectifier

Rating specification of the FCSC-rectifier	
Parameters	Specifications
Input voltage	Variable three-phase RMS (phase-neutral), 75-100 V
Input frequency	Variable frequency of 240-480 Hz
Load power	1 kW

Main components employed in the 1 kW FCSC-rectifier			
Symbol	Manufacturer	Part Number	Typical data
C_C	General Electric	97F8248 (Polypropylene film)	8 µF, 660 V AC
S_1-S_6	IXYS	IXDR 30N120	1200 V, 50 A
D_1-D_6	IXYS	VU062-16NO7	1600 V, 63 A
C_L	Panasonic	EETEE2W251LJ (Electrolytic type)	2 × 250 µF, 450 V

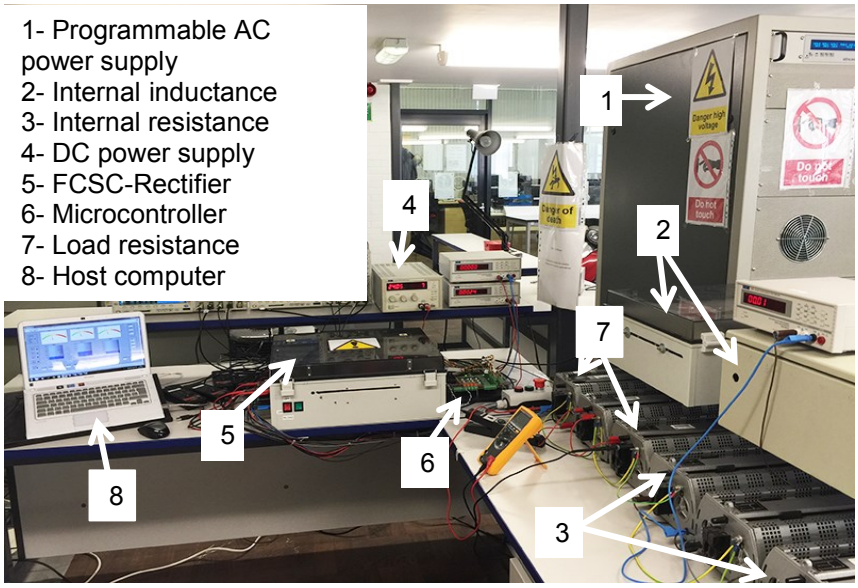

Fig. 12. Photograph of the experimental test rig.

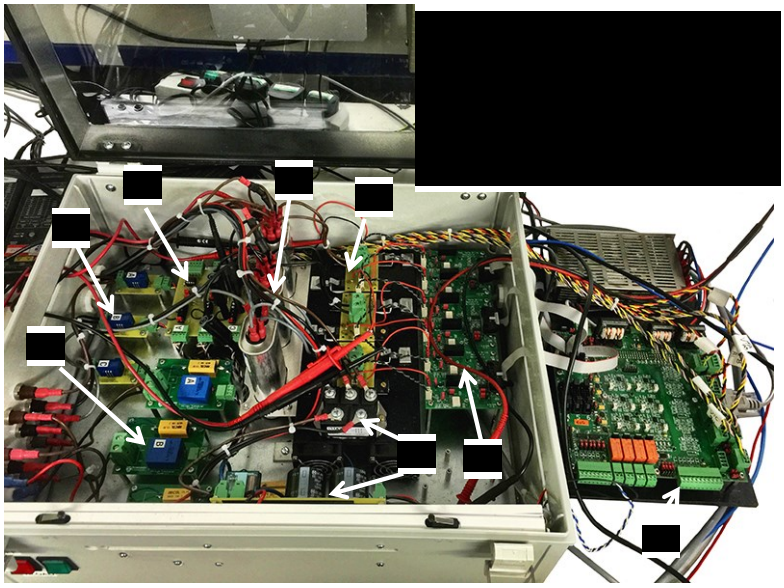

Fig. 13. Photograph of the FCSC-rectifier.

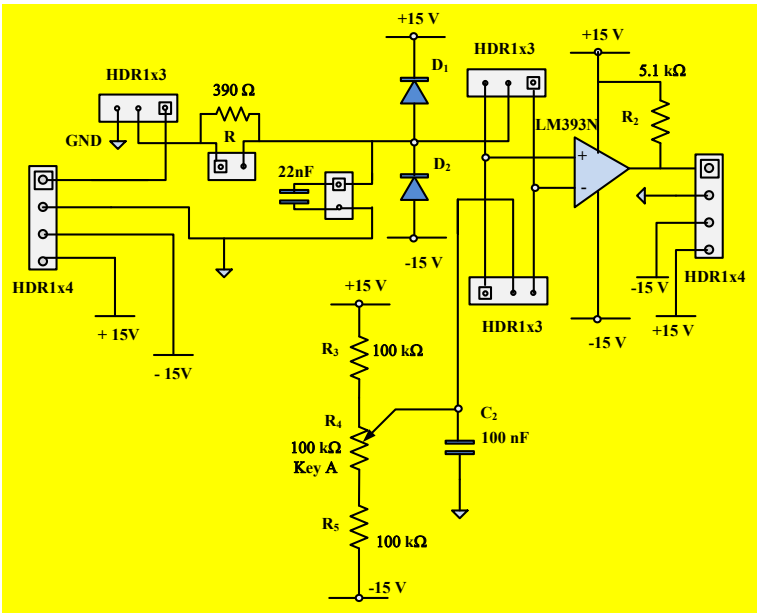

Fig. 14 Zero-crossing detection circuit

Fig. 15 shows the recorded experimental results for operation at typical aircraft frequency of 400 Hz and a voltage of 90V. Waveforms for line-to-neutral supply voltage V_s, the input current i_s, DC load voltage V_L, and DC load current I_L are shown, as well as the voltage across the series capacitor V_{CC} and the pulses supplied to the switches S_1 and S_2 through one dual driving circuit board. The supply current is almost sinusoidal with an RMS value of about 3.5 A, and is practically in-phase with the supply voltage v_s confirming the effectiveness of the control strategy in matching the effective capacitive reactance to the generator inductive reactance. The dc load voltage is constant at 160 V because of the presence of the load capacitor C_L. The figure also shows the switch timing pulses and the resulting series capacitor voltage, which is zero when S_1 or S_2 are closed in each half-cycle of the supply voltage waveform.

The same system behavior is observed when comparing simulation and experimental results, however, the experimental results show differences in the magnitudes of voltage and current compared with simulations. For example, the load voltage in Fig. 15 is 130 V (experimental) whereas the load voltage in Fig. 10 is 170 V (simulation). The highest errors between simulation and experimental values occur at the highest voltage and frequency of 100V/480Hz with a 22.9% difference in the values of average load voltage V_L. This error decreases at lower frequencies. The differences can be explained by the extra losses in the experimental test circuit due to the use of passive components (inductors L_S and series capacitors C_C) designed to be employed at 50 Hz. To support this statement the FCSC-rectifier was operated at 50V/50Hz. The error between measurement and simulation at 50 Hz was reduced in this case to below 5%. This confirms that inductor core loss and capacitor losses in the test rig are responsible for the discrepancy between experimental and simulated results when operated at frequencies above 50 Hz. This observation has been previously reported [44] in power factor correction applications with switching converters. An accurate calculation of inductor loss is highly challenging in applications where the frequency or the duty cycle are variable since conventional methods for core loss

estimation based on manufacturer's data sheets cannot be used in such cases. In an aircraft installation the PM generator will be specifically designed to operate over the required range of frequencies and care will be taken to reduce machine losses to a minimum. For example in [42] and [45] core losses are reduced by using a segmented stator PM alternator to reduce the magnetic wedges which effect the eddy current loss.

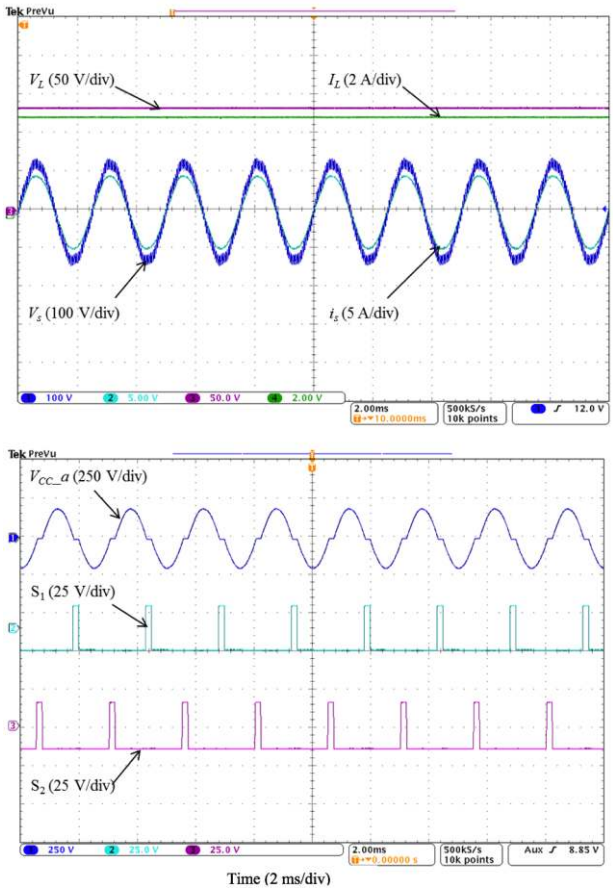

Fig. 15. Experimental FCSC-rectifier waveforms at 90V/400 Hz.

Fig. 16 shows the measured relationship between power factor, load and voltage/frequency. This figure clearly shows that the input power factor is high at all values of supply voltage and frequency. The highest power factor (0.99) was achieved at the higher voltage/frequency of 100V/480Hz. The minimum value of power factor (0.95) occurred at minimum load, recorded at 75V/240Hz. The figure also shows that the variation in load resistance has a small impact on the power factor.

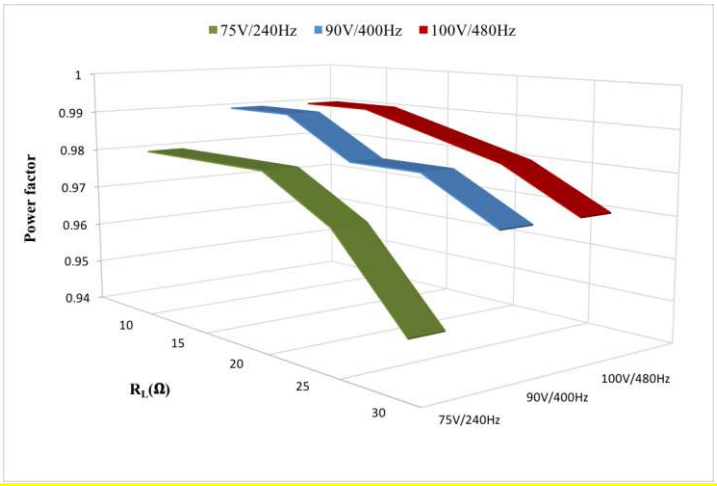

Fig. 16. FCSC-rectifier power factor as a function of PM generator voltage and frequency under various load conditions (experimental results).

VI. Harmonic and Efficiency Analysis

Since the three-phase FCSC-rectifier is being proposed for aircraft applications, it is imperative to examine the AC current harmonic spectrum as a function of load variations. This is important due to the strict limits placed on individual harmonics in such applications. In this section, the harmonic components of the simulated and experimental AC current waveforms are calculated using FFT analysis, up to the 40th harmonic as required in MEA standards. Results are compared with the demands imposed by DO-160G as listed in [26] to examine the suitability of the FCSC-rectifier in an aircraft application. Harmonic spectra are presented at minimum voltage/frequency and at maximum voltage/frequency. In addition, operation at two load conditions R_L = 20 Ω and R_L = 10 Ω (emulates a load change of 50%).

A. Harmonic Spectrum (Simulation results)

Fig. 17 compares simulation results at 100V/480Hz and 75V/240Hz with DO-160G for a load of R_L = 20 Ω. All the current harmonics at both frequencies are lower than the specified limits. The same observation is made when the load resistor value is halved (Fig. 18).

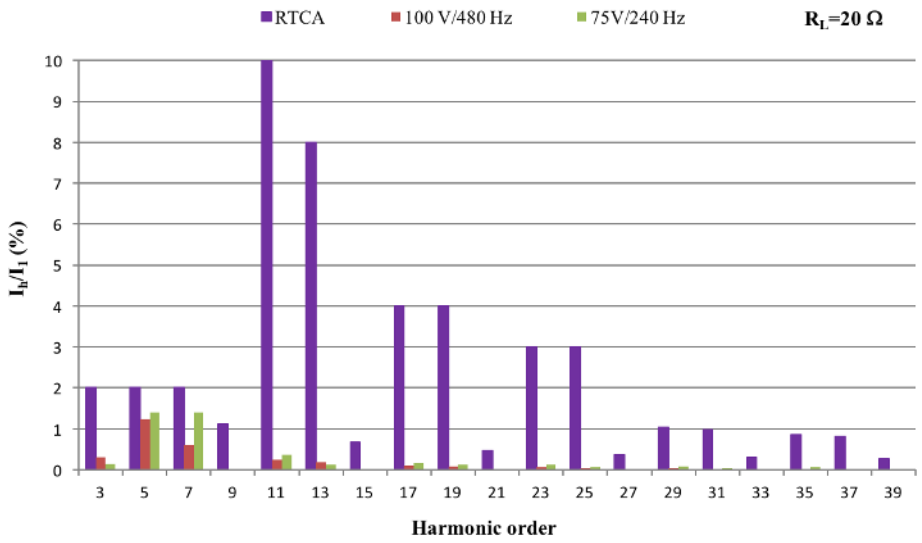

Fig. 17. Input current harmonic spectrum as a function of V_S/f_S; simulated waveforms, R_L= 20 Ω.

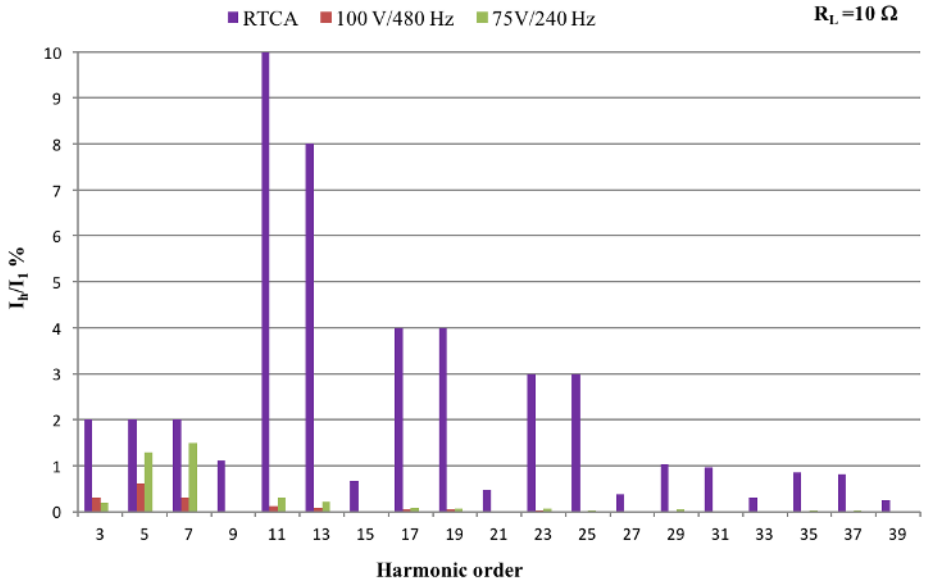

Fig. 18. Input current harmonic spectrum as a function of V_S/f_S; simulated waveforms R_L= 10 Ω

B. Harmonic Spectrum (Experimental results)

Similarly, Fig. 19 shows that none of the individual harmonics exceed DO-160G limits while operating the test rig with a load resistance of R_L =20 Ω. Fig. 20 illustrates the effect of reducing the load resistor to 10 Ω. Reassuringly, all current harmonics are below DO-160G specifications. The case of 480Hz and R_L *=10 Ω* represents maximum power delivered to the load. The IGBT stress at this condition is 16.5 A collector peak current and 687 V maximum collector-emitter voltage which is equal to the capacitor voltage V_{cc}.

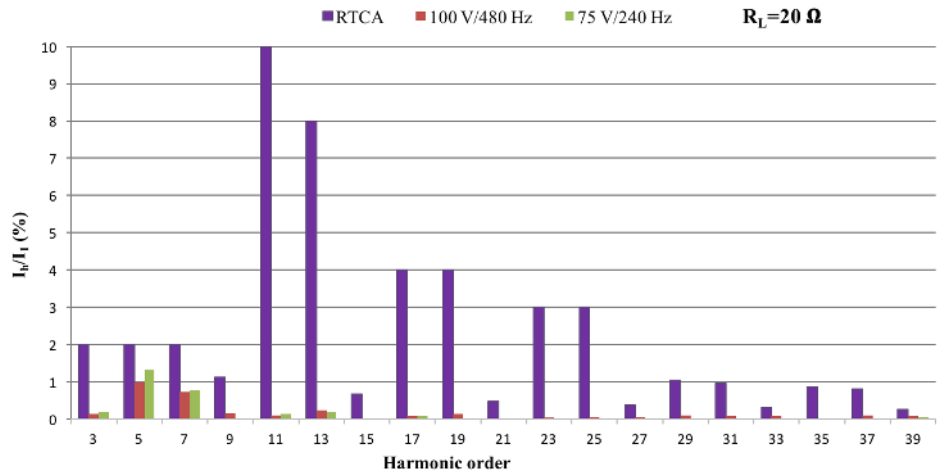

Fig. 19. Input current harmonic spectrum as a function of V_S/f_S; experimental waveforms, R_L= 20 Ω

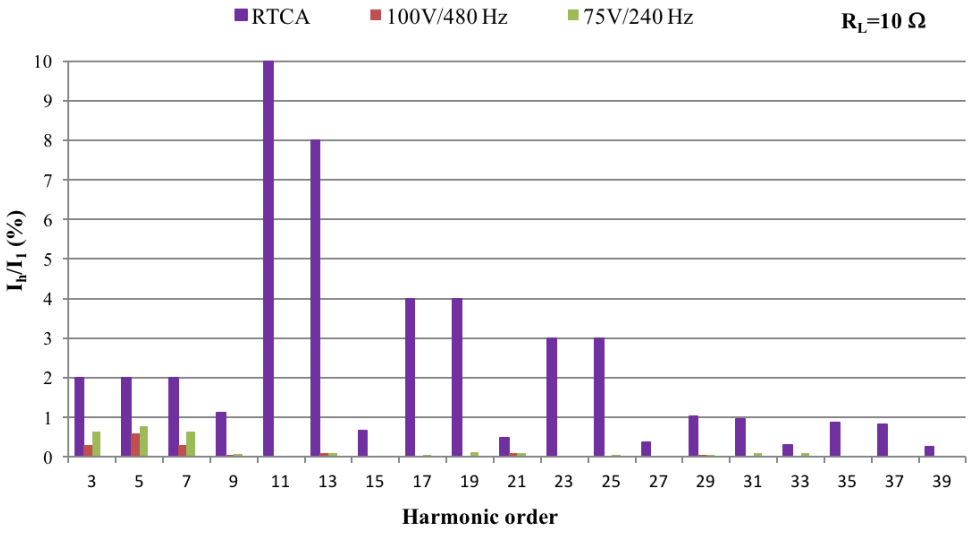

Fig. 20. Input current harmonic spectrum as a function of V_S/f_S; experimental waveforms, R_L= 10 Ω

C. Efficiency Analysis

The FCSC-rectifier experiences on-state losses from the IGBTs (S1 to S6) and diodes (D1 to D6), and resistive losses caused by the internal parasitic resistors of the three capacitors (Cc). IGBT on-state losses occur only during the conduction period δ, thus the on-state losses for one IGBT can be expressed as:

$$P_{IGBT} = \frac{\delta}{2\pi} * I_{ph} * V_{CE\ on-state} \qquad (14)$$

where I_{ph} is the phase RMS current and $V_{ce\ on\text{-}state}$ is the on-state voltage of the IGBT. Switching losses can be ignored as the switching frequency for each IGBT is half the supply frequency f_s. Each of the diodes conducts for a period of π, thus the on-state losses for one diode is:

$$P_{diode} = \frac{\pi}{2\pi} * I_{ph} * V_{on-state} = \frac{I_{ph} * V_{on-state}}{2} \qquad (15)$$

with $V_{on\text{-}state}$ being the on-state voltage of the diode. The capacitor has a resistance of 66mΩ, thus ohmic losses of the capacitor Cc can be estimated to:

$$P_C = \frac{2\pi-\delta}{2\pi} * I_{ph}^2 * R_c \qquad (16)$$

Based on (14-16), total FCSC-rectifier losses were calculated (P_{total}) for four different scenarios as shown in Table 5. Corresponding efficiency figures (η_{cal}) are also included in the table, calculated from the output powers for each scenario, showing efficiency values between 95% and 98.6%. The Table also includes measured efficiency values (η_m); approximately 2% lower than the calculated efficiencies.

Table 5. FCSC-rectifier losses and efficiencies at different operating conditions

Load	Supply voltage/frequency	δ	P_{total}	η_{cal}	η_m
R_L=10Ω	100V/480Hz	0.00°	54.27 W	97.87%	94.16%
	75V/240Hz	86.41°	67.91 W	95.09%	92.60%
R_L=20Ω	100V/480Hz	0.00°	25.17 W	98.55%	95.31%
	75V/240Hz	86.41°	35.57 W	96.23%	93.40%

VII. Conclusion

This paper proposes a three-phase, variable-frequency, variable-voltage FCSC-rectifier circuit for MEA applications that does not require any filters in order to comply with current harmonics regulations such as DO-160G. The proposed rectifier is ideal for stand-alone systems such as powering the FADEC onboard an aircraft. The rectifier incorporates an IGBT controlled, three-phase series compensation circuit connected between a PM synchronous generator and a diode bridge rectifier. The reactance of the capacitor is continually varied (in line with the varying supply frequency) to match the generator inductive reactance and to achieve a minimum impedance resonant condition. This results in a sinusoidal AC current waveform in phase with the generator induced voltage over a wide range of operational voltages and frequencies.

Simulation and experimental results clearly show that the FCSC-rectifier is able to maintain a high value of power factor over a wide range of voltage and frequencies values at different load conditions. The power factor improves with increasing load and supply frequency. All individual harmonics fell within the allowable limits when tested over a range of frequencies from 480 Hz to 240 Hz. This occurred at all load conditions without the need for any additional filtering. In principal, the FCSC-rectifier can also be employed for other stand-alone aircraft VFG systems whenever there is a requirement for powering aircraft systems independently from an auxiliary power unit, as well as other stand-alone systems in non-aircraft applications.

References

[1] B. Sarlioglu and C. T. Morris, "More Electric Aircraft: Review, Challenges, and Opportunities for Commercial Transport Aircraft," *IEEE Transactions on Transportation Electrification*, vol. 1, pp. 54-64, June 2015.

[2] X. Roboam, B. Sareni and A. D. Andrade, “More Electricity in the Air: Toward Optimized Electrical Networks Embedded in More-Electrical Aircraft,” *IEEE Industrial Electronics Magazine*, vol. 6, no. 4, pp. 6-17, Dec 2012.

[3] J. Rosero, J. Ortega, E. Aldabas and L. Romeral, “Moving towards a more electric aircraft,” *IEEE Aerospace and Electronic Systems Magazine*, vol. 22, no. 3, March 2007.

[4] K. Peng, D. Fan, F. Yang, M. He, Y. Wang and F. She, "Development and Test Evaluation of Full Authority Digital Electronic Control System for Auxiliary Power Unit Based on Electronic Pump, " in *IEEE Int. Conf. on Signal Processing, Communication and Computing (ICSPCC),* 2016, pp. , Hong Kong. China.

[5] K. Beneda, " Development of a Modular FADEC for Small Scale Turbojet Engine, "In *IEEE Int. Symposium on Applied Machine Intelligence and Informatics(SAMI),* 2016, PP. 51-56, Herlany, Slovakia.

[6] C. Cao, J. Shen, M. Luo, B. Yu, J. Wang and Z. Hu, " FWorks: An Integrated digital simulation platform for FADEC systems, " in *IEEE Chinese Control Conference (CCC*), 2017, pp. 10316-10321, Dalian, China.

[7] I. Moir, and A. Seabridge, Aircraft Systems: mechanical, electrical, and avionics subsystems integration, John Wiley & Sons, 2008.

[8] B. Chen, C. Li, Y. Li and A. Wang, "Reliability analysis method of an aircraft engine FADEC system," in *International Conference on Reliability, Maintainability and Safety*, 2009, pp. 289-292, Chengdu, China.

[9] L. Stoica, V. Solomko, T. Baumheinrich, R. Del Regno, R.Beigh, S. Riches, I. White, G. Rickard, P. Williams, "Design of a high temperature signal conditioning ASIC for engine control systems - HIGHTECS," in *IEEE Int. Symposium on Circuits and Systems (ISCAS)*, 2014, pp. 2117-2120, Melbourne, Australia.

[10] J. Lutambo, J. Wang, H. Yue and G. Dimirovsky, "Aircraft turbine engine control systems development: Historical Perspective," in *IEEE Chinese Control Conference (CCC*), 2015, Hangzhou, China.

[11] Sean Gallagher, 2015, available at https://arstechnica.co.uk/information-technology/2015/06/report-airbus-transport-crash-caused-by-wipe-of-critical-engine-control-data.

[12] J. P. Morris and F. R. Lysinger, “Power source for aircraft engine controller systems” U.S. Patent 11 899 053, March, 2009.

[13] P. Wheeler and S. Bozhko, “The More Electric Aircraft: Technology and challenges,” *IEEE Electrification Magazine,* vol. 2, no. 4, pp. 6-12, Dec 2014.

[14] H. Abu-Rub, M. Malinowski and K. Al-Haddad, Power Electronics for Renewable Energy Systems, Transportation and Industrial Applications, West Sussex: IEEE Press, Wiley, 2014.

[15] K. Emadi and M. Ehsani, “Aircraft power systems: technology, state of the art, and future trends,” *IEEE Aerospace and Electronic Systems Magazine*, vol. 15, no. 1, pp. 28-32, Jan 2000.

[16] A. J. Mitcham and J. J. A. Cullen, "Permanent magnet generator options for the More Electric Aircraft," in *Int. Conference on Power Electronics, Machines and Drives*, 2002, pp. 241-245, Sante Fe, NM, USA.

[17] C. R. Avery, S. G. Burrow and P. H. Mellor, “Electrical generation and distribution for the more electric aircraft,” in *42nd Int. Universities Power Engineering Conference (UPEC)*, 2007, pp.1007-1012, Brighton, UK.

[18] D. M. Miao, Y. Mollet, J. Gyselinck and J. X. Shen, "DC Voltage Control of a Wide-Speed-Range Permanent-Magnet Synchronous Generator System for More Electric Aircraft Applications," in *IEEE Vehicle Power and Propulsion Conference (VPPC)*, 2016, pp. 1-6, Hangzhou, China.

[19] J. Chen, X. Zhang and C. Wen, “Harmonics Attenuation and Power Factor Correction of a More Electric Aircraft Power Grid Using Active Power Filter,” *IEEE Transactions on Industrial Electronics*, vol. 63, no. 12, pp. 7310-7319, Dec 2016.

[20] “Enviromental conditions and test procedures for airborne equipment, DO-160G,” RTCA, Inc, Washington DC, 2004.

[21] J. Sun, "Conducted EMI modeling and mitigation for power converters and motor drives," in ESA Workshop on Aerospace EMC, 2012, pp. 1-6, Venice, Italy.

[22] J. Brombach, M. Jordan, F. Grumm and D. Schulz, “Converter topology analysis for aircraft application,” in *Int. Symp. on Power Electronics Electrical Drives Automation and Motion (SPEEDAM)*, 2012, 446-451, Sorrento, Italy.

[23] A. Mallik and A. Khaligh, "Comparative study of three-phase buck, boost and buck-boost rectifier topologies for regulated transformer rectifier units," in *IEEE Transportation Electrification Conference and Expo (ITEC)*, 2015, pp. 1-7, Dearborn, MI, USA.

[24] A. Mallik, B. Faulkner and A. Khaligh, “Control of a Single-Stage Three-Phase Boost Power Factor Correction Rectifier,” in *IEEE Applied Power Electronics Conference and Exposition (APEC)*, 2016, pp.54-59, Long Beach, CA, USA.

[25] X. Zhao, J. M. Guerrero and X. Wu, “Review of aircraft electric power systems and architectures,” in *IEEE Int. Energy Conference (ENERGYCON)*, 2014, pp. 949-953, Cavtat, Croatia.

[26] A. O. Monroy, L.-H. Hoang and C. Lavoie, "Modelling and simulation of a 24-pulse Transformer Rectifier Unit for more electric aircraft power system," in Electrical Systems for Aircraft, Railway and Ship Propulsion (ESARS), 2012, pp. 1-5, Bologna, Italy.

[27] F. Meng, L. Gao, S. Yang, W. Yang, “Effect of phase-shift angle on a delta-connected autotransformer applied to a 12-pulse rectifier,” IEEE Trans. Ind. Electron., vol. 62, no. 8, pp. 4678-4690, June 2015.

[28] B. Sarlioglu, “Advances in AC-DC power conversion topologies for More Electric Aircraft,” in IEEE Transportation Electrification Conference and Expo (ITEC), 2012, pp. 1-6C Dearborn, MI, USA.

[29] T. Yang, S. Bozhko and G. Asher, "Active front-end rectifier modelling using dynamic phasors for more-electric aircraft applications," in IET Electrical Systems in Transportation, vol. 5, no. 2, pp. 77-87, June 2015.

[30] G. Gong, M. L. Heldwein, U. Drofenik, J. Minibock, K. Mino and J. W. Kolar, “Comparative evaluation of three-phase high-power-factor AC-DC converter concepts for application in future More Electric Aircraft,” in *IEEE Transactions on Industrial Electronics*, vol. 52, pp. 727-737, June 2005.

[31] D. Y. Komovskiy, "Comparative analysis of three-level PWM inverters for aircraft AC power systems," in 17th *International Conference of Young Specialists on Micro/Nanotechnologies and Electron Devices* (EDM), 2016, pp. 476-480, Erlagol, Russia.

[32] M. Liserre, F. Blaabjerg, and S. Hansen, “Design and control of an LCL filter-based three-phase active rectifier,” *IEEE Trans. Ind. Appl.*, vol. 41, no. 5, pp. 1281–1291, Sep./Oct. 2005.

[33] K. Jalili and S Bernet, “Design of LCL Filters of Active-Front-End Two-Level Voltage-Source Converters,” *IEEE Trans. Ind Appl.*, vol. 56, no. 5, pp1674-1689, May 2005

[34] L. F. W. de Souza, E. H. Watanabe and J. E. da Rocha Alves, “Thyristor and Gate-Controlled Series Capacitors: A Comparison of Components Rating,” *IEEE Transactions on Power Delivery,* vol. 23, no. 2, pp. 899-906, April 2008.

[35] F. D. de Jesus, E. H. Watanabe, L. F. W. de Souza and J. E. R. Alves, “SSR and Power Oscillation Damping Using Gate-Controlled Series Capacitors (GCSC),” *IEEE Transactions on Power Delivery*, vol. 22, no. 3, pp. 1806-1812, July 2007.

[36] H. A. Mohammadpour, M. M. Islam, E. Santi and Y. J. Shin, "SSR Damping in Fixed-Speed Wind Farms Using Series FACTS Controllers," *IEEE Transactions on Power Delivery*, vol. 31, no. 1, pp. 76-86, Feb. 2016.

[37] I. Matsumoto and S. Nomura, "Power factor correction of large current line commutated converters using variable series capacitors," *2013 15th European Conference on Power Electronics and Applications (EPE)*, 2013, pp. 1-9, Lille, France.

[38] N. G. Hingorani and L. Gyugyi, Understanding FACTS: concepts and technology of flexible AC transmission system. New York: IEEE Press, 2000.

[39] R. Hunter and G Elliot, Wind-Diesel Systems: A Guide to the Technology and Its Implementation, Cambridge University Press, 1994.

[40] T. Al-Mhana, V. Pickert and B. Zahawi, "FCSC converter with symmetrical short duty cycle for variable frequency applications," *7th IET International Conference on Power Electronics, Machines and Drives (PEMD 2014)*, 2014, pp. 1-5, Manchester, UK.

[41] T. Al-Mhana, B. Zahawi and V. Pickert, "Symmetrical duty cycle control for FCSC converter for wave energy applications," *2014 9th International Symposium on Communication Systems, Networks & Digital Sign (CSNDSP)*, Manchester, 2014, pp. 56-60, Manchester, UK.

[42] NJ Baker, DJ Smith, MC Kulan and S Turvey, “Design and performance of a Segmented Stator Permanent Magnet Alternator for Aerospace,” IEEE Trans. on Energy Conversion, Early Access, 2017

[43] NJ Baker, DJ Smith, MC Kulan and S Turvey, “Design and performance of a segmented stator permanent magnet alternator for aerospace,” IET International Conference on Power Electronics, Machines and Drives (PEMD 2014), 2014, pp. 1-5, Manchester, UK

[44] L. Jinjun, T. G. Wilson, R. C. Wong, R. Wunderlich and F. C. Lee, "A method for inductor core loss estimation in power factor correction applications," in *17th IEEE Applied Power Electronics Conference and Exposition (APEC)* 2002, pp. 439-445, Dallas, TX, USA.

[45] W.U.N. Fernando M. Barnes O. Marjanovic, “Direct drive permanent magnet generator fed AC–DC active rectification and control for more-electric aircraft engines,” IET electric power applications, Vol. 5, 2011.